Acta Crystallographica Section A
Foundations of Crystallography
ISSN 0108-7673

Received 23 April 2001
Accepted 1 September 2001

Concerning intensity profiles

Elisabeth Rossmanith

Mineralogisch-Petrographisches Institut der Universität Hamburg, D-20146 Hamburg, Grindelallee 48, Germany. Correspondence e-mail: rossmanith@mineralogie.uni-hamburg.de

The kinematical derivation of intensity profiles is considered. It is shown that the shapes of the profiles depend not only on the shape of the crystal but also on the crystal system and axial ratios of the unit cell and on the angles between the direction of the diffracted beam and the cell axes. For all crystal shapes, the widths of the profiles are determined by the Lorentz factor and the mean thickness of the crystal in the direction of the diffracted beam. The similarity of the intensity distributions of cubiform and spherical crystals is discussed. It is shown that almost identical results are obtained for the kinematical intensity profiles of a plane parallel plate having a large crystal edge ratio bathed in the beam and the dynamical profiles of thin plane parallel plates with infinite lateral extension. Extinction-corrected profiles of the plane parallel plate are compared with the results of the dynamical theory. In the case of a spherical crystal, the primary-extinction correction factor, y_p, obtained with extinction-corrected profiles is compared with y_p commonly used in structure analysis.

1. Introduction

In §§2.1 and 2.2 of Authier & Malgrange (1998) (cited as A&M hereafter), the intensity profiles obtained in the framework of the kinematical theory are compared with those obtained according to the dynamical approach. Extinction is discussed in §2.3. Some of the formulae and statements presented in these paragraphs are misleading. Although the shape dependence of the intensity profile is discussed in §2.1 of A&M, the shape-dependent path lengths of the incident and reflected beams, which determine the maximum value of the intensity distribution, are missing in the expression given for the intensity profile, I_h. As a consequence, I_h has an unusual dimension, the profiles have to be presented in Fig. 2 of A&M in a 'normalized' form, which masks similarities in the shapes between the kinematical and dynamical profiles, and the 'integrated intensity' obtained by integrating I_h over the scanning variable differs appreciably from the expression given in textbooks.

The detailed analysis of the kinematical interference functions, developed in the 1930s and 1940s (see, for example, Patterson, 1939), has possibly fallen into oblivion to a large extent. It seems worthwhile, therefore, to present in the following a short review of the derivation of the kinematical intensity profiles for crystals of various shapes using the modern tool *Mathematica* (Wolfram, 1999), to make supplementary remarks on dynamical results and to compare the kinematical expressions with dynamical, as well as extinction-corrected, intensity distributions. Although several equations given in this paper can be found in textbooks or in previous papers of the author, the basic results are summarized in §2 in order to aid the reader in following the derivation of the new expressions.

In §2, the shape-independent expressions for the intensity profile, the width of the profile, the maximum value of the profile and the integrated intensity are derived. Then the profiles for a parallelepipedon and a sphere are given explicitly. The dependence of the profile shape on the angle between the direction of the diffracted beam and the unit-cell axes is discussed. Profiles of crystal spheres and platelets bathed in the incident beam are presented. In §3, results of the dynamical theory are summarized. In §4, extinction-corrected profiles given in the literature are compared with the dynamical reflectivity distributions. Last, but not least, the primary-extinction correction obtained with the extinction-corrected profiles is compared with extinction corrections commonly used in structure analysis.

2. Kinematical intensity profiles

In the framework of the kinematical theory, the intensity diffracted elastically in the direction $\mathbf{k}_i \equiv MP_i$ (Fig. 1; P_i are particular surface points on the Ewald sphere with radius $|k_0| = |k_i| = 1/\lambda$ and centre M, λ is the wavelength of the incident and reflected beams and H is a reciprocal-lattice point) is given by (Azaroff, 1968)

$$I_{P_i} = (I_0 p/R^2) r_0^2 F^2 G^2 = (I_0 p/R^2) r_0^2 F^2 (V_{\rm cry}/V_{\rm cell})^2 G_1^2. \quad (1)$$

I_0 is the incident intensity [energy cm^{-2} s^{-1}], p is the polarization factor equal to 1 and $(\cos 2\theta)^2$ for the parallel and perpendicular components of the X-ray electric field, respectively (in the case of unpolarized or partly polarized beams the usual mean values have to be calculated), R is the distance between the crystal and the detector, r_0 is the classical electron radius, F is the structure factor, $V_{\rm cry}$ is the crystal volume, $V_{\rm cell}$

is the unit-cell volume and G is the interference function. G^2 is proportional to the square of the number of unit cells in the crystal, N, and to the crystal-shape-dependent distribution function G_1^2. The maximum value of G_1^2 is equal to unity and the volume integral in reciprocal space is given by

$$\int G_1^2 \, \mathrm{d}V^* = 1/V_{\mathrm{cry}}.$$

The power crossing the detector surface [energy s^{-1}] is obtained by integrating the intensities diffracted in the particular directions $\mathbf{k}_i$ over the area A of the detector surface

$$\int I_{P_i} \, \mathrm{d}A = R^2 \lambda^2 \int I_{P_i} \, \mathrm{d}S, \qquad (2)$$

where $\mathrm{d}S$ is the area element on the Ewald sphere perpendicular to the direction of the diffracted beam. For simplicity, it is assumed that the locus of the points P_i in Fig. 1, *i.e.* the section area S between the Ewald sphere and the G_1^2-dependent surroundings of the reciprocal-lattice point, can be approximated by a plane. Using the mean thickness $\bar{t}_{\mathrm{in}}$ of the crystal defined by $\bar{t}_{\mathrm{in}} = V_{\mathrm{cry}}/q_{\mathrm{in}}$, where q_{in} is the cross section of the crystal normal to the incident beam, and the abbreviation $1/\Lambda = r_0 \lambda |F| p^{1/2}/V_{\mathrm{cell}}$, equation (2) can be expressed as

$$R(\zeta)_{\mathrm{kin}} = \frac{I(\zeta)}{I_0 q_{\mathrm{in}}} = \frac{1}{I_0 q_{\mathrm{in}}} \int I_{P_i} \, \mathrm{d}A = \frac{\bar{t}_{\mathrm{in}}}{\Lambda^2} V_{\mathrm{crys}} \int G_1^2(\zeta) \, \mathrm{d}S. \qquad (3)$$

The dimensionless reflectivity $R(\zeta)_{\mathrm{kin}}$ therefore depends on the values of the distribution function G_1^2 in the section area S, *i.e.* it depends on ζ, the distance between the Ewald sphere and the reciprocal-lattice point H in the direction of the reflected beam (see Fig. 1). The intensity profile $I(\zeta)/I_0 q_{\mathrm{in}}$ is obtained, pulling the reciprocal-lattice point together with its surroundings in the direction of the diffracted beam from outside to inside the Ewald sphere ['pull down procedure' (Rossmanith, 2000*a*), cited as Ro00*a* hereinafter]. Bearing in mind that $\mathrm{d}S\mathrm{d}\zeta = \mathrm{d}V^*$, where $\mathrm{d}\zeta$ is the element in the direction of the reflected beam, the total 'integrated intensity' [energy s^{-1} cm^{-1}] obtained during the 'pull down procedure', *i.e.* the area of the profile, is proportional to the volume integral in the reciprocal space,

$$\frac{I^{(\zeta)}_{\mathrm{integral}}}{(I_0 q_{\mathrm{in}})} = \frac{\bar{t}_{\mathrm{in}}}{\Lambda^2} V_{\mathrm{cry}} \iint G_1^2 \, \mathrm{d}S \, \mathrm{d}\zeta = \frac{\bar{t}_{\mathrm{in}}}{\Lambda^2}. \qquad (4)$$

The maximum of the profile corresponds to (3) calculated for $\zeta = 0$. Consequently the fundamental quantity in profile analysis, the integral widths $\Delta\zeta_{\mathrm{integral}}$ of the profile, defined as the width of a rectangle with the same maximum and the same area [equation (20.5) of Azaroff (1968)], is the quotient of expressions (4) and (3),

$$\Delta\zeta_{\mathrm{integral}} = 1/\left[V_{\mathrm{crys}} \int G_1^2(\zeta = 0) \, \mathrm{d}S\right] = 1/\bar{t}_{\mathrm{diffr}}. \qquad (5)$$

It is clear from (3) and (5) that $\bar{t}_{\mathrm{diffr}} = 1/\Delta\zeta_{\mathrm{integral}}$ has dimensions of length, *i.e.* it is an average of the thickness of the crystal in the direction of the diffracted beam. The maximum of the dimensionless reflectivity profile $I(\zeta)/I_0 q_{\mathrm{in}}$ can therefore be expressed as

$$I(\zeta = 0)/I_0 q_{\mathrm{in}} = \bar{t}_{\mathrm{in}} \bar{t}_{\mathrm{diffr}}/\Lambda^2. \qquad (6)$$

For intermediate Bragg angles, the section areas **S** corresponding to the 'pull down procedure' differ only marginally from the section areas **S** corresponding to the ω scan (rotation about the axis perpendicular to the plane of the paper through the zero point of the reciprocal space), *i.e.* assuming that the circular path of the reciprocal lattice point can be approximated by a straight line in the vicinity of the Ewald sphere, the profiles obtained during the ω-scan are equivalent to those obtained during the 'pull down procedure'. The profiles differ only in their abscissae and the dimensions of the corresponding variable. It was shown in Ro00*a* that the integral width $\Delta\omega_{\mathrm{integral}}$ of an intensity profile obtained using the ω-scanning technique is given by (Ro00*a*-16)

$$\Delta\omega_{\mathrm{integral}} = \Delta\zeta_{\mathrm{integral}} \lambda L \cong \lambda/(\bar{t}_{\mathrm{diffr}} \sin 2\theta_{\mathrm{B}}), \qquad (7)$$

where L is the Lorentz factor. The expressions (1)–(7) are valid for all crystal shapes.

For a crystal having the shape of a parallelepipedon whose sides are parallel to the cell edges,

$$G_1^2 = \frac{1}{(N_1 N_2 N_3)^2} \left[\frac{\sin(\pi N_1 x^*)}{\sin(\pi x^*)} \frac{\sin(\pi N_2 y^*)}{\sin(\pi y^*)} \frac{\sin(\pi N_3 z^*)}{\sin(\pi z^*)}\right]^2 \qquad (8)$$

is obtained (Fig. 2), where x^*, y^*, z^* are the components of any vector $\mathbf{d}^* = x^*\mathbf{a}^* + y^*\mathbf{b}^* + z^*\mathbf{c}^*$ in reciprocal space, $\mathbf{a}^*$, $\mathbf{b}^*$, $\mathbf{c}^*$ are the reciprocal-lattice vectors and N_1, N_2, N_3 are the numbers of unit cells lying along the edges of the crystal. The total number of unit cells in the parallelepipedon is therefore $N = N_1 N_2 N_3$. The interference function is therefore a periodic function with intensity maxima in the surrounding of the reciprocal-lattice points. It should be noted that, as in the case of the dynamical theory, all reciprocal-lattice points contribute to the diffracted intensity (making possible simultaneous diffraction), although the contribution of lattice points far away from the Ewald sphere will be negligibly small.

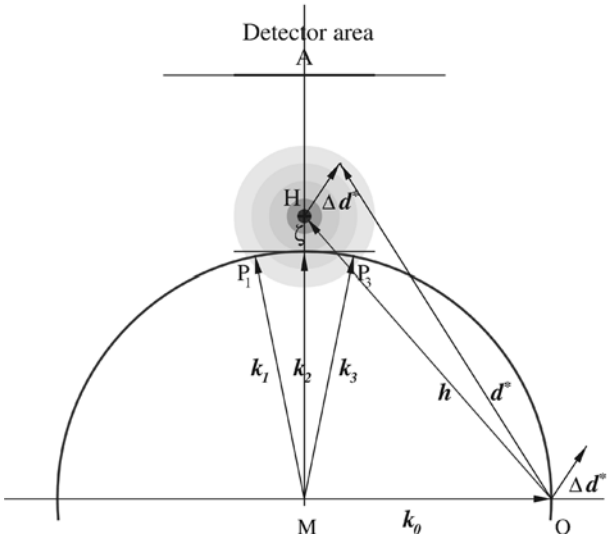

Figure 1
The geometry of the 'pull down procedure' in reciprocal space.

Because of the periodicity of the distribution function G_1^2, any vector $\mathbf{d}^*$ can be replaced by the vector $\mathbf{\Delta d}^* = \mathbf{d}^* - \mathbf{h} = \Delta x^*\mathbf{a}^* + \Delta y^*\mathbf{b}^* + \Delta z^*\mathbf{c}^*$ (see Fig. 1), where $\mathbf{h}$ is a vector connecting the origin of the reciprocal lattice with a reciprocal-lattice point H, *i.e.* the components x^*, y^*, z^* in (8) can be replaced by the components Δx^*, Δy^*, Δz^*. For the sake of (8) being integrable, the *sines* in the denominator of the periodic function are usually replaced by their arguments resulting in a function which is no longer periodic in reciprocal space (Fig. 3*a*). For a rectangular parallelepipedon, the numbers N_i can be calculated according to $a_{\rm crys}a^*$, $b_{\rm crys}b^*$, $c_{\rm crys}c^*$, where $a_{\rm crys}$, $b_{\rm crys}$, $c_{\rm crys}$ and a^*, b^*, c^* are the lengths of the edges of the crystal and the lengths of the reciprocal-lattice vectors, respectively. Introducing the variables $\zeta_x = a^*\Delta x^*$, $\zeta_y = b^*\Delta y^*$, $\zeta_z = c^*\Delta z^*$, (8) can be approximated by

$$G_1^2 \cong \left[\frac{\sin(\pi a_{\rm crys}\zeta_x)}{\pi a_{\rm crys}\zeta_x}\frac{\sin(\pi b_{\rm crys}\zeta_y)}{\pi b_{\rm crys}\zeta_y}\frac{\sin(\pi c_{\rm crys}\zeta_z)}{\pi c_{\rm crys}\zeta_z}\right]^2. \qquad (9)$$

The distribution functions shown in Figs. 2 and 3(*a*) were calculated for a crystal cube ($a_{\rm crys} = b_{\rm crys} = c_{\rm crys}$) consisting of $N = 1000$ cubic unit cells ($a^* = b^* = c^*$).

In the case of a spherically shaped crystal with a cubic lattice and radius r, it was shown, for example, by Wilson (1962), that G_1^2 can be approximated by

$$G_1^2 \cong \left[3\frac{\sin(2\pi\varepsilon r) - 2\pi\varepsilon r\cos(2\pi\varepsilon r)}{(2\pi\varepsilon r)^3}\right]^2, \qquad (10)$$

where ε is defined by $\varepsilon = (\zeta_x^2 + \zeta_y^2 + \zeta_z^2)^{1/2}$. The lattice function shown in Fig. 3(*b*) was calculated for a spherical crystal, of radius $r = [3/(4\pi)Na_{\rm cell}^3]^{1/3} \equiv 0.62a_{\rm crys}$, where $a_{\rm cell} = 1/a^*$ is the lattice constant of the spherical as well as the cubiform crystal. In Fig. 3(*c*), the profiles of the two functions (9) and (10), obtained for $\zeta_y = \zeta_z = 0$, are compared. It is obvious from Fig. 3 that the main maxima of cubiform and spherical crystals, both having the same crystal volume $V_{\rm crys} = Na_{\rm cell}^3$, are very similar in shape. The distribution functions differ appreciably only for the higher-order maxima. In the case of the spherical crystal, the neighbourhood of the reciprocal-lattice point is spherically symmetric, whereas in the case of the cubiform crystal, whose sides are parallel to the cell edges, the intensity of the higher-order maxima is concentrated along the reciprocal axes. Furthermore, the contour plots of G_1^2 calculated for the

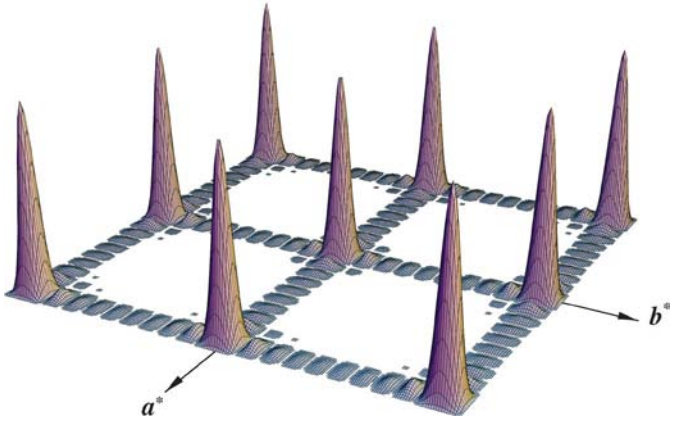

Figure 2
G_1^2 for a cubiform crystal with edges $a_{\rm crys}$ (arbitrary units) parallel to the cubic unit-cell edges. G_1^2 was calculated according to (8) by means of *Mathematica*. $N_1 = N_2 = N_3 = 10$, $\zeta_z = 0$; ζ_x, ζ_y, ζ_z having the dimensions (units of $a_{\rm crys})^{-1}$.

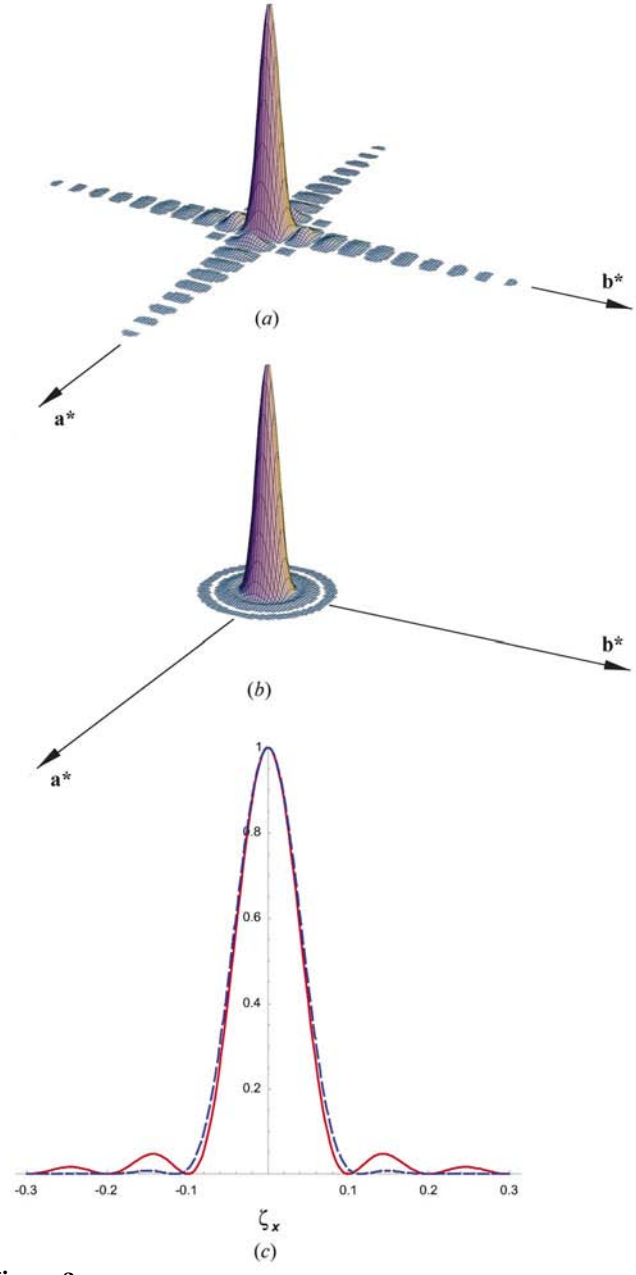

Figure 3
(*a*) G_1^2 for a cubiform crystal with edges $a_{\rm crys}$ (arbitrary units) parallel to the cubic unit-cell edges. G_1^2 was calculated according to expression (9) by means of *Mathematica*. $N_1 = N_2 = N_3 = 10$, $\zeta_z = 0$; ζ_x, ζ_y, ζ_z having the dimensions (units of $a_{\rm crys})^{-1}$. (*b*) G_1^2 for a spherical crystal with cubic unit cell and with $r \equiv 0.62a_{\rm crys}$ (*i.e.* 0.62 times the edges of the cubiform crystal of *a* and Fig. 2). G_1^2 was calculated according to expression (10) by means of *Mathematica*, $\zeta_z = 0$. (*c*) G_1^2 calculated by means of *Mathematica* for $\zeta_y = \zeta_z = 0$ for a cubiform crystal [expression (9), red solid line] and a spherical crystal [expression (10), blue dashed line], the two crystals having the same volume.

cubiform crystal with edges a_{crys} and shown in Figs. 5(*a*) and 5(*b*) can be compared with the contour plot of a rectangular plane parallel plate with edges $c_{crys} = b_{crys} = 5a_{crys}$, represented in Fig. 4(*a*).

In the case when the plane of diffraction is restricted to the (*hk*0) plane in reciprocal space (*i.e.* $\mathbf{k}_0$ and $\mathbf{k}$ in the plane of the paper), for the rectangular parallelepipedon the length $\bar{t}_{diffr} = 1/\Delta\zeta_{integral}$ will depend on the angle φ between the unit-cell edge a_{crys} [*i.e.* ζ_x in Fig. 4(*a*)] and the vector in the direction of the diffracted beam, $\mathbf{k}$. In the cases $\varphi = 0$ and $\varphi = 90°$, the two orthogonal coordinate systems attached to the crystal (ζ_x, ζ_y, ζ_z) and to the diffracted beam, $\mathbf{k}$ (k_x antiparallel to the diffracted beam, k_z parallel to ζ_z, k_y in the plane **S**), respectively, are parallel. Using the transformation $\zeta_x = k_x \cos\varphi - k_y \sin\varphi$, $\zeta_y = k_x \sin\varphi + k_y \cos\varphi$, and bearing in mind that for the peak maximum $k_x = \zeta = 0$, the length $\bar{t}_{diffr}(\varphi) = 1/\Delta\zeta_{integral}(\varphi)$ can be calculated according to

$$\bar{t}_{diffr}(\varphi) = a_{crys} b_{crys} c_{crys} \int_{-\infty}^{+\infty} \left[\frac{\sin(\pi a_{crys}\zeta_x)}{\pi a_{crys}\zeta_x}\right]^2 \times \left[\frac{\sin(\pi b_{crys}\zeta_y)}{\pi b_{crys}\zeta_y}\right]^2 \left[\frac{\sin(\pi c_{crys}\zeta_z)}{\pi c_{crys}\zeta_z}\right]^2 dk_y\, d\zeta_z. \quad (11)$$

For $\varphi = 0$ and 90°, it follows that $\zeta_x = k_x = 0$ and $\zeta_y = k_x = 0$, respectively. It can therefore easily be shown that, for $\varphi = 0°$, equation (11) results in $\bar{t}_{diffr}(\varphi) = a_{crys}$, whereas, for $\varphi = 90°$, the result $\bar{t}_{diffr}(\varphi) = b_{crys}$ is obtained, *i.e.* in these two cases the length $\bar{t}_{diffr}(\varphi)$ corresponds to the constant thickness of the crystal in the direction $\mathbf{k}$. Furthermore, by means of *Mathematica*, for $0 < \varphi < 90°$, the length $\bar{t}_{diffr}(\varphi)$ can be given as an analytical expression,

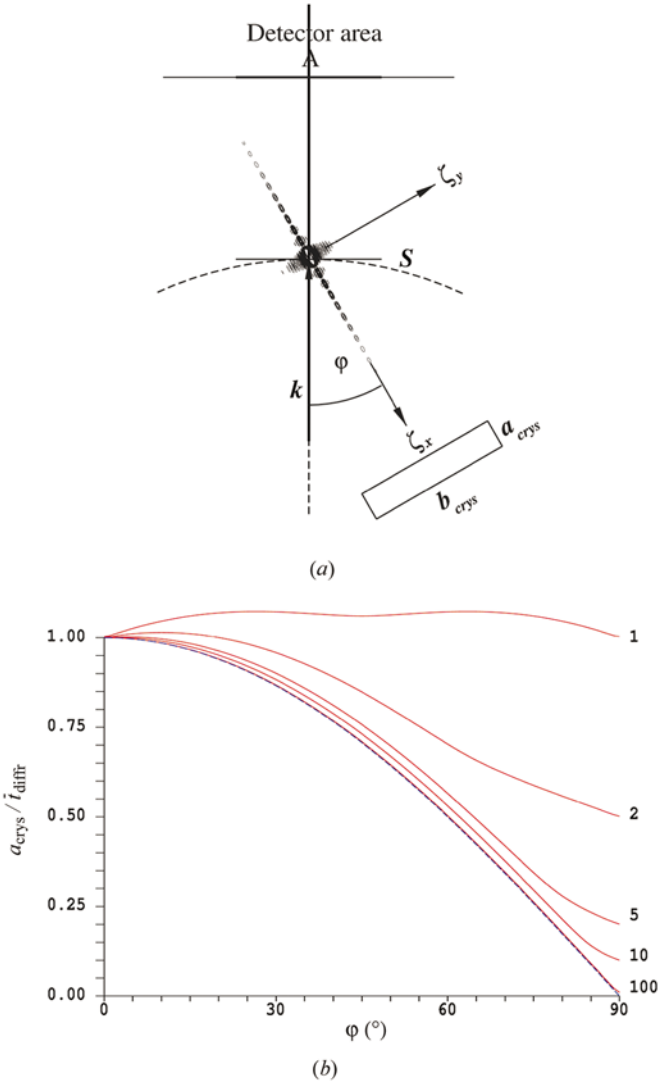

Figure 4
(*a*) The geometry of diffraction in the (*hk*0} plane of the reciprocal space. Surrounding of the reciprocal-lattice point corresponds to the rectangular parallelepipedon with edges parallel to the cubic unit-cell edges. $N_1 = 10$, $N_2 = N_3 = 50$. (*b*) Red lines: $a_{crys}/\bar{t}_{diffr}(\varphi)$ calculated according to expression (12) for different crystal edge length $b_{crys} = na_{crys}$, with $n = 1, 2, 5, 10, 100$. Blue dashed line: $a_{crys}/\bar{t}_{diffr}(\varphi) = \cos\varphi$.

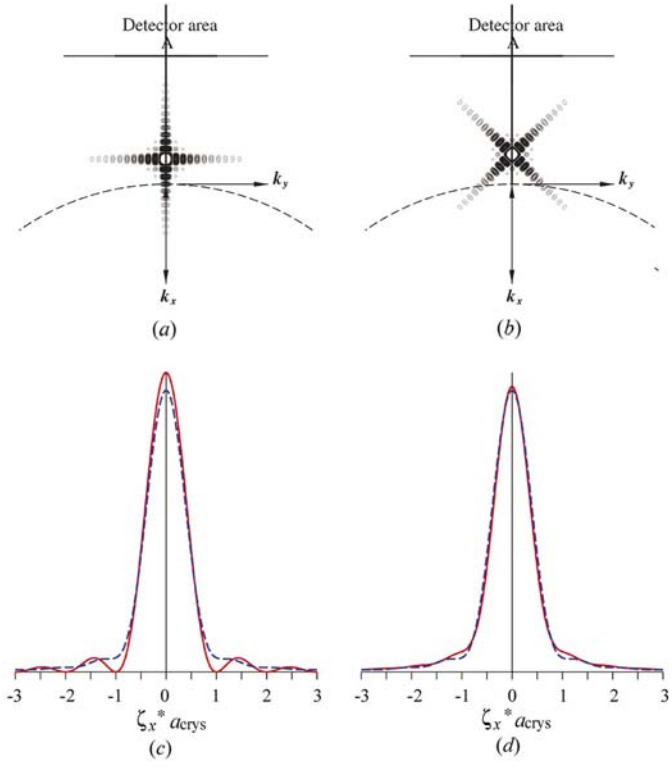

Figure 5
(*a*) $\varphi = 0°$ and (*b*) $\varphi = 45°$. The geometry of diffraction in the (*hk*0) plane of the reciprocal space. Surrounding of the reciprocal-lattice point corresponds to the cubiform crystal with edges a_{crys} parallel to the cubic unit-cell edges. $N_1 = N_2 = N_3 = 10$. (*c*) $\varphi = 0°$ and (*d*) $\varphi = 45°$. $I(\zeta)/\text{const} = \int G_1^2(\zeta)\, dS$. Red solid lines: cubiform crystal ($a_{crys} = b_{crys} = c_{crys}$). Blue dashed lines: spherical crystal. Both crystals consist of the same substance, have the same volume and are bathed in the same incident beam. The constant is therefore identical for the two samples.

$$\bar{t}_{\rm diffr} = \big[-2(b_{\rm crys}\pi\cos\varphi)^3 - 2(a_{\rm crys}\pi\sin\varphi)^3 + \big|b_{\rm crys}\pi\cos\varphi - a_{\rm crys}\pi\sin\varphi\big|^3 + \big|b_{\rm crys}\pi\cos\varphi + a_{\rm crys}\pi\sin\varphi\big|^3\big] \times (6a_{\rm crys}b_{\rm crys}\pi^3\sin^2\varphi\cos^2\varphi)^{-1}. \quad (12)$$

In the case when the diffraction plane is not restricted to the (*hk*0) plane in reciprocal space, the expression for $\bar{t}_{\rm diffr}$, and as a consequence $\Delta\omega_{\rm integral}$ [expression (7)], will become even more complicated. In Fig. 4(*b*), the ratio $a_{\rm crys}/\bar{t}_{\rm diffr}(\varphi)$, calculated according to (12), is plotted *versus* the angle φ for different crystal edge length $b_{\rm crys} = na_{\rm crys}$, with n = 1, 2, 5, 10, 100. It is obvious from the figure that for large edge-length ratios the $a_{\rm crys}/\bar{t}_{\rm diffr}(\varphi)$ curve approaches the blue dashed curve in Fig. 4(*b*), which corresponds to $a_{\rm crys}/\bar{t}_{\rm diffr}(\varphi) = \cos\varphi$.

In Fig. 5, the intensity profiles

$$I(\zeta)/\text{constant} = \int G_1^2(\zeta)\,{\rm d}S$$

obtained for $\varphi = 0$ (Figs. 5*a* and 5*c*) and 45° (Figs. 5*b* and 5*d*) are compared for a cubiform ($a_{\rm crys} = b_{\rm crys} = c_{\rm crys}$, red solid lines) and a spherical crystal (blue dashed lines), both crystals consisting of the same substance, having the same volume and bathed in the same incident beam. The constant is therefore identical for the two samples. In the case shown in Figs. 5(*a*) and 5(*c*) with ζ_x antiparallel to the direction of the reflected beam and ζ_y, ζ_z in the plane S, $\bar{t}_{\rm diffr} = a_{\rm crys}$. In the case shown in Figs. 5(*b*) and 5(*d*), expression (12) results in $\bar{t}_{\rm diffr} = (2\sqrt{2}/3)a_{\rm crys} \cong 0.94a_{\rm crys}$ (see also Fig. 4*b*). It was shown in Ro00*a* that, for a spherical crystal, $\bar{t}_{\rm diffr} = 3r/2 \cong 0.93a_{\rm crys}$ is obtained. The heights $I(\zeta = 0)$ [expression (6)] and the integral widths [expression (5)] of cubiform and spherical crystals having the same volume are therefore almost identical. Furthermore, in the case of Fig. 5(*d*), the two profiles are very similar in shape.

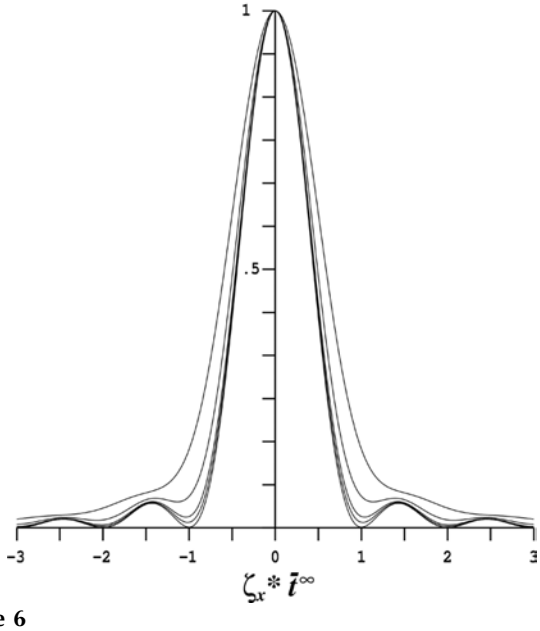

Figure 6
$I(\zeta)/I(\zeta = 0)$ calculated for $\varphi = 45°$ for plane parallel plates all with the same volume, $V_{\rm crys} = 1$, *versus* $\zeta^*\bar{t}^{\infty}$. Crystal edge ratios, n = 1, 2, 5, 10, 100 from outermost to innermost curve ($a_{\rm crys} = n^{-2/3}$ = 1, 0.63, 0.34, 0.22, 0.046; $b_{\rm crys} = na_{\rm crys}$ = 1, 1.26, 1.7, 2.2, 4.6; $\bar{t}^{\infty} = a_{\rm crys}/\cos\varphi$ = 1.41, 0.89 0.48, 0.3, 0.066 in arbitrary units).

In Fig. 6, intensity profiles $I(\zeta)/I(\zeta = 0)$ calculated for φ = 45° for plane parallel plates all with the same volume, $V_{\rm crys} = 1$, but having different crystal edge ratios, $b_{\rm crys} = c_{\rm crys} = na_{\rm crys}$ (n = 1, 2, 5, 10, 100 from outermost to innermost curve, *i.e* $a_{\rm crys} = n^{-2/3}$ = 1, 0.63, 0.34, 0.22, 0.046; $b_{\rm crys} = na_{\rm crys}$ = 1, 1.26, 1.7, 2.2, 4.6; $\bar{t}^{\infty} = a_{\rm crys}/\cos\varphi$ = 1.41, 0.89 0.48, 0.3, 0.066, all lengths in arbitrary units), are plotted *versus* $\zeta^*\bar{t}^{\infty}$, where $\bar{t}^{\infty}$ corresponds to the (constant) thickness (= beam path length in the direction of the diffracted beam) of a plane parallel plate with infinite lateral extension (blue dashed line in Fig. 4).

It is evident from Fig. 6 that with increasing edge ratio, n, the *kinematical profile* of the plane parallel plate *bathed in the beam* becomes more and more similar in shape to the profile of the plane parallel plate with *infinite lateral extension*, presented in Fig. 7(*a*) (dashed black line), calculated according to expression (15), *the 'kinematical approximation' obtained in the framework of the dynamical theory*, which will be discussed in the following two sections. It should be noted, however, that, in a routine experiment with a beam cross section of about 0.5 mm, an edge ratio, $n > 100$, of a crystal bathed in the beam would require a crystal plate with edges $b_{\rm crys}$ and $c_{\rm crys} <$ 0.5 mm and, consequently, $a_{\rm crys} < 5$ µm, *i.e.* it would require a crystal with a shape which would be difficult to obtain.

It is evident that expressions (3), (5) and (6) become extremely complicated for a crystal with triclinic symmetry, arbitrary shape and arbitrary diffraction plane, whereas (4) does not depend on these features.

3. Dynamical intensity profiles

For simplicity, the expressions given for the power ratio, $R_{\rm dyn}$, are restricted to non-absorbing crystals, *i.e.* $(F_hF_{-h})^{1/2} = F_h$, and to symmetrical reflection, *i.e.* the reflecting plane is parallel to the surface of the plane parallel plate with unlimited lateral extension. Consequently, the thickness of the crystal in the direction of the incident beam is equal to the thickness in the diffracted beam, $\bar{t}_{\rm in} = \bar{t}_{\rm diffr} = \bar{t}^{\infty}$. In the framework of the dynamical theory, expressions for $R_{\rm dyn}$ are given, for example, by Zachariasen (1945), here referred to as Z45. Replacing Zachariasen's symbol A defined in (Z45-3.140) by $A \equiv \bar{t}^{\infty}/\Lambda$ and replacing the symbol y defined in (Z45-3.141) by $y \equiv \pi\Lambda\zeta$, the following expressions are obtained. For the Bragg case,

$$R(\zeta)_B = \frac{1}{(\pi\Lambda\zeta)^2 + [(\pi\Lambda\zeta)^2 - 1]\cot^2\{(\bar{t}_B^{\infty}/\Lambda)[(\pi\Lambda\zeta)^2 - 1]^{1/2}\}} \quad \text{for} \quad (\pi\Lambda\zeta)^2 > 1 \qquad \text{(Z45-3.143)}$$

$$R(\zeta)_B = \frac{1}{(\pi\Lambda\zeta)^2 + [1 - (\pi\Lambda\zeta)^2]\coth^2\{(\bar{t}_B^{\infty}/\Lambda)[1 - (\pi\Lambda\zeta)^2]^{1/2}\}} \quad \text{for} \quad (\pi\Lambda\zeta)^2 < 1 \qquad \text{(Z45-3.144).} \quad (13)$$

For the Laue case,

$$R(\zeta)_L = (\bar{t}_L^{\infty}/\Lambda)^2 \left\{ \frac{\sin[(\pi \bar{t}_L^{\infty}\zeta)^2 + (\bar{t}_L^{\infty}/\Lambda)^2]^{1/2}}{[(\pi \bar{t}_L^{\infty}\zeta)^2 + (\bar{t}_L^{\infty}/\Lambda)^2]^{1/2}} \right\}^2, \quad \text{(Z45-3.142)} \qquad (14)$$

where $\bar{t}_B^{\infty} = t_0/\sin\theta_B$ (Bragg case) and $\bar{t}_L^{\infty} = t_0/\cos\theta_B$ (Laue case) and t_0 is the thickness of the plate normal to the plate surface, where θ_B is the Bragg angle. For the sake of clarity in Fig. 7, the peak shift term in Zachariasen's y, which is zero for the Laue case, is neglected in the Bragg case.

For thin crystals, (13) and (14) can be approximated by [see Fig. 7(*a*), discussed in the following section]

$$R(\zeta)_{\rm kin} \simeq (\bar{t}^{\infty}/\Lambda)^2 \left[\frac{\sin(\pi \bar{t}^{\infty}\zeta)}{\pi \bar{t}^{\infty}\zeta} \right]^2, \quad \text{(Z45-3.157)} \qquad (15)$$

the 'kinematical approximation' obtained in the framework of the dynamical theory, where $\bar{t}^{\infty} = \bar{t}_B^{\infty}$ in the Bragg case and $\bar{t}^{\infty} = \bar{t}_L^{\infty}$ in the Laue case.

4. Extinction-corrected intensity profiles

Extinction-corrected intensity profiles derived in the framework of the kinematical theory for different crystal shapes are given by Zachariasen (1967) (here referred to as Z67) and Becker & Coppens (1974) (here referred to as B&C).

Exact solutions of the Hamilton–Darwin transfer equations for the plane parallel plate with unlimited lateral extension were presented by Z67 and reconsidered by B&C. According to B&C's expression (26), the kinematical reflectivity for this case is given by (15) (B&C's symbols ε_1 and α are equivalent to $\omega = \zeta\lambda L$ and $\bar{t}^{\infty}/\lambda L$, respectively, *i.e.* $\varepsilon_1\alpha = \zeta\bar{t}^{\infty}$). Using (Z67-12) and (Z67-13), the extinction-corrected reflectivities for the symmetrical Bragg case,

$$R(\zeta)_B^{\rm ext} = R(\zeta)_{\rm kin}/[1 + R(\zeta)_{\rm kin}], \qquad (16)$$

and the symmetrical Laue case,

$$R(\zeta)_L^{\rm ext} = \{1 - \exp[-2R(\zeta)_{\rm kin}]\}/2, \qquad (17)$$

are obtained. In Fig. 7, the dynamical profiles obtained according to (13) (red line) and (14) (blue line), given in the figure only for $\zeta < 0$, are compared with the profile (15) (black dashed line) as well as with the extinction-corrected profiles (16) (red line) and (17) (blue line). The last three profiles are presented only for $\zeta > 0$. For $\bar{t}^{\infty}/\Lambda = 0.3$ (Fig. 7*a*), the profiles are very similar in shape, and the heights of the profiles, $R(\zeta=0)_B = 0.0849$, $R(\zeta=0)_L = 0.0873$, $R(\zeta=0)_{\rm kin} = 0.09$, $R(\zeta=0)_B^{\rm ext} = 0.0826$ and $R(\zeta=0)_L^{\rm ext} = 0.0824$, differ only slightly. The dashed black profile is almost identical in shape with the innermost profile of Fig. 6. For $\bar{t}^{\infty}/\Lambda = 1$ (Fig. 7*b*), the extinction-corrected profiles are poor approximations of the dynamical profiles.

As pointed out by Rossmanith (2000*b*) (hereafter Ro00*b*), owing to energy conservation the diffracted intensity cannot be larger than the intensity incident on the crystal sample, *i.e.* there exists an upper limit for the kinematical reflection profile defined by $R(\zeta)_{\rm upperlimit} = R(\zeta)_{\rm kin}$ for $R(\zeta)_{\rm kin} < 1$ and $R(\zeta)_{\rm upperlimit} = 1$ otherwise. Therefore, in the cases of Figs. 7(*c*) and 7(*d*), *i.e.* for $\bar{t}^{\infty}/\Lambda = 3$ and 10, corresponding to $R(\zeta=0)_{\rm kin} = 9$ and $R(\zeta=0)_{\rm kin} = 100$, respectively, the kinematical profile (15) is replaced by $R(\zeta)_{\rm upperlimit}$. Nevertheless, for these large $\bar{t}^{\infty}/\Lambda$ ratios (Figs. 7*c* and 7*d*), no agreement between the dynamical and extinction-corrected kinematical profiles is obtained. One possible reason for this disagreement may be the inappropriate experimental condition – an infinite plane parallel plate cannot be bathed in the incident beam. As a consequence, the volume $V_{\rm crys}$ involved in the diffraction process is clearly defined only for the case where the incident and diffracted beams are exactly parallel ($2\theta = 0$ or 180°: $\bar{t}_{\rm in} = \bar{t}_{\rm diffr} = \bar{t}^{\infty}$, $q_{\rm in} = q_{\rm diffr}$, where $q_{\rm diffr}$ is the beam cross section of the diffracted beam). For all other cases, *i.e.* during the ω scan and even more for intermediate Bragg angles, the volume $V_{\rm crys} = \bar{t}_{\rm in}q_{\rm in}$ will not be identical to the volume $\bar{t}_{\rm diffr}q_{\rm diffr}$. In agreement with B&C, '*it must be concluded that the transfer equations incorrectly describe the primary extinction effect in an infinite parallel plate*'.

In the case of a perfect spherical crystal bathed in the incident beam, the extinction-corrected reflectivity profiles given by B&C are defined by

$$R(\zeta)_{\rm sphere}^{\rm ext} = R(\zeta)_{\rm kin}\varphi_{\rm B\&C}, \qquad (18)$$

where $R(\zeta)_{\rm kin}$, defined by the expression (Ro00*b*-8),

$$R(\zeta)_{\rm kin} = \frac{\bar{t}_{\rm in}\bar{t}_{\rm diffr}}{\Lambda^2} \frac{1 + 8(\pi r\zeta)^2 - \cos(4\pi r\zeta) - 4\pi r\zeta\sin(4\pi r\zeta)}{32(\pi r\zeta)^4} = 4\sigma r/3, \qquad (19)$$

is proportional to the diffracting cross section per unit volume and unit intensity, σ, defined by (B&C-29). In (19), $\bar{t}_{\rm in} = V_{\rm crys}/q_{\rm in} = (4/3)r$ and $\bar{t}_{\rm diffr} = (3/2)r = 9/8\bar{t}_{\rm in}$ [expressions (Ro00*a*-6) and (Ro00*a*-11)]. A closed form for $\varphi_{\rm B\&C}$ could be given by B&C only for the two cases [$2\theta = 180^\circ$, *i.e.* the 'Bragg case'; the obvious printing error, *i.e.* interchange of the sign '+' and the fraction '1/2', is corrected here, otherwise (B&C-32) would not correspond to the series expansion (B&C-33*a*)]

$$\varphi_{\rm B\&C}(2\theta = 180^\circ) = \frac{3}{4(\sigma r)^3}\left[(\sigma r)^2 - \sigma r + \tfrac{1}{2}\ln(1 + 2\sigma r)\right] \qquad \text{(B\&C-32)}$$

and ($2\theta = 0^\circ$, *i.e.* the 'Laue case')

$$\varphi_{\rm B\&C}(2\theta = 0^\circ) = \frac{3}{64(\sigma r)^3}\left\{8(\sigma r)^2 + 4\sigma r\exp(-4\sigma r) - [1 - \exp(-4\sigma r)]\right\}. \qquad \text{(B\&C-1)}$$

In Fig. 8, the extinction-corrected profiles $R(\zeta)_{\rm sphere}^{\rm ext}$ for the 'Bragg case' (red line) as well as the 'Laue case' (blue line) are compared with the kinematical profile $R(\zeta)_{\rm kin}$ (black line). The maxima of the kinematical profiles in Fig. 8 are given by $R(\zeta)_{\rm kin}^{\rm max} = (9/8)(\bar{t}_{\rm in}/\Lambda)^2$, *i.e.* in Fig. 8(*a*) [(*b*), (*c*), (*d*)] with $\bar{t}_{\rm in}/\Lambda = 0.3$ [1, 3, 30], $R(\zeta)_{\rm kin}^{\rm max} = 0.101$ (1.125, 10.125, 1012.5). Therefore, in the representation of Figs. 8(*b*), 8(*c*) and 8(*d*), the kinematical profiles whose maxima exceed the value 1 are replaced by $R(\zeta)_{\rm upperlimit}$ corresponding to (19). It is obvious from Fig. 8 that, in agreement with energy conservation, for large $\bar{t}_{\rm in}/\Lambda$ ratios the maxima of B&C's extinction-corrected

profiles approach $R(\zeta = 0)^{\rm ext}_{\rm sphere} = 1$ in the 'Bragg case'. In the 'Laue case', the maxima are limited to 1/2. Furthermore, it should be noted that the area of the extinction-corrected profiles is considerably smaller than the area of the profiles $R(\zeta)_{\rm upperlimit}$.

It seems worthwhile therefore to compare the extinction correction, obtained with these profiles, with extinction corrections commonly used in crystallographic software. According to (B&C-7), the primary extinction factor, y_p, is defined as the ratio of the area of the extinction-corrected profile to the area of the kinematical profile (see also Ro00*b*-§2.3). Using the profiles defined in (18) and (19), the extinction correction

$$y_p = \int R(\zeta)_{\rm kin}\varphi_{\rm B\&C}\,{\rm d}\zeta \Big/ \int R(\zeta)_{\rm kin}\,{\rm d}\zeta, \qquad (20)$$

as well as the extinction-corrected mean thickness of the crystal, $t_{\rm ext} = \bar{t}_{\rm in} y_p$, expression (Ro00*b*-13),

$$t_{\rm ext} = \Lambda^2 \int R(\zeta)_{\rm kin}\varphi_{\rm B\&C}\,{\rm d}\zeta, \qquad (21)$$

can be calculated for B&C's 'Bragg case' as well as 'Laue case' for increasing values of the mean thickness of the crystal, $\bar{t}_{\rm in}$. The results (curve 3: 'Bragg case'; curve 4: 'Laue case') are presented in Fig. 9 for $\Lambda = 1$ (arbitrary units), *i.e.* $\bar{t}_{\rm in}$ as well as $t_{\rm ext}$ are given in units of Λ. The 'upper limit' of $t_{\rm ext}$ for a spherical crystal (curve 2), corresponding to the profiles $R(\zeta)_{\rm upperlimit}$ (expression Ro00*b*-12) is also given. The dynamical result for the extinction-corrected mean thickness of a semi-infinite plate, $t_{\rm ext} = \Lambda \tanh(\bar{t}^{\,\infty}/\Lambda)$ (expression Ro00*b*-6) is presented as curve 1. The dotted curves in Fig. 9, on the other hand, represent the results obtained with B&C's analytical expression for y_p,

$$y_p = \Big\{1 + 2(\tfrac{3}{2}r^2/\Lambda^2) + A(\theta_B)(\tfrac{3}{2}r^2/\Lambda^2)^2 \times [1 + B(\theta_B)(\tfrac{3}{2}r^2/\Lambda^2)]^{-1}\Big\}^{-1/2}, \qquad \text{(B\&C.37)}$$

calculated for various Bragg angles θ_B, with $A(\theta_B) = 0.2 + 0.45\cos 2\theta_B$ and $B(\theta_B) = 0.22 - 0.12(0.5 - \cos 2\theta_B)^2$.

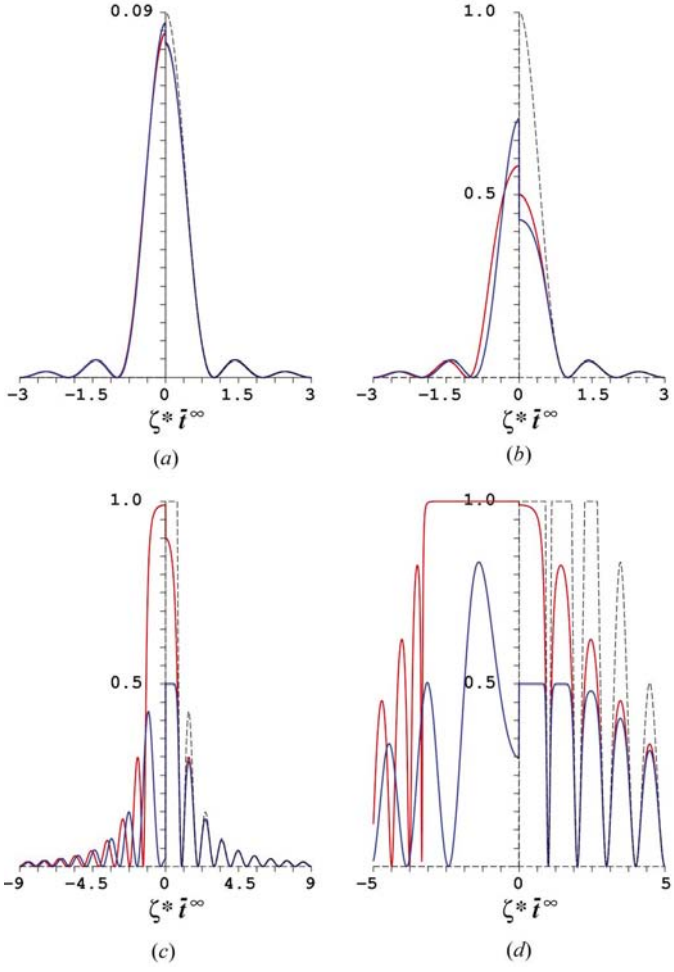

Figure 7
Comparison of dynamical and kinematical profiles for a plane parallel plate with infinite lateral extension. For $\zeta < 0$, red line: dynamical Bragg case, expression (13); blue line: dynamical Laue case, expression (14). For $\zeta > 0$, black dashed line: profile $R(\zeta)_{\rm upperlimit}$ corresponding to (15); red line: extinction-corrected kinematical profile, expression (16); blue line: extinction-corrected kinematical profile, expression (17). (*a*) $\bar{t}^{\,\infty}/\Lambda = 0.3$; (*b*) $\bar{t}^{\,\infty}/\Lambda = 1$; (*c*) $\bar{t}^{\,\infty}/\Lambda = 3$; (*d*) $\bar{t}^{\,\infty}/\Lambda = 10$.

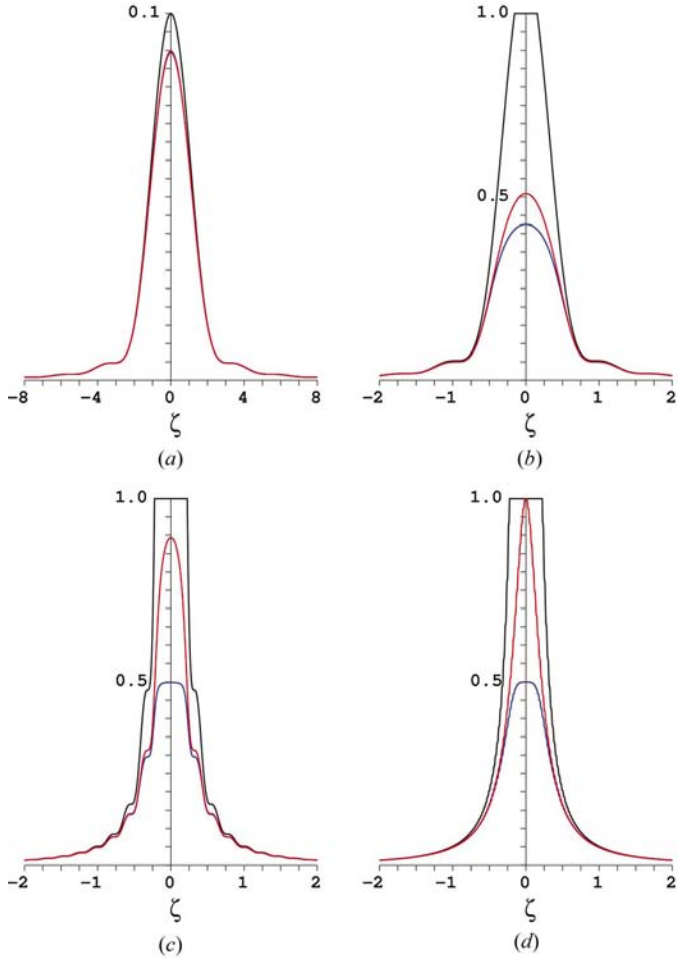

Figure 8
Comparison of the extinction-corrected profiles $R(\zeta)^{\rm ext}_{\rm sphere}$ with $R(\zeta)_{\rm upperlimit}$ for a spherical crystal. Red line: 'Bragg case' ($2\theta = 180^\circ$). Blue line: 'Laue case' ($2\theta = 0^\circ$). Black line: $R(\zeta)_{\rm upperlimit}$ corresponding to (19). (*a*) $\bar{t}_{\rm in}/\Lambda = 0.3$. (*b*) $\bar{t}_{\rm in}/\Lambda = 1$. (*c*) $\bar{t}_{\rm in}/\Lambda = 3$. (*d*) $\bar{t}_{\rm in}/\Lambda = 30$.

As a result of the complete reflection of the incident beam in large crystals, for all $\bar{t}_{in}/\Lambda$ ratios, the extinction length Λ is obviously an upper limit for the extinction-corrected mean thickness of the crystal, t_{ext}. This is true for the plane parallel plate considered in the framework of the dynamical theory (curve 1) as well as for the spherical crystal considered in the framework of the kinematical approach (curves 2, 3 and 4). The extinction-corrected thickness of a crystal, t_{ext}, obtained with B&C's 'Bragg case' profiles (curve 3) is considerably smaller than t_{ext} corresponding to curve 2. The large difference between curves 2 and 3 can readily be explained by the much smaller areas of B&C's 'Bragg case' profiles compared with the $R(\zeta)_{upperlimit}$ profiles (see Fig. 8), the areas of the latter being definitely overestimated. It is interesting to note that B&C lines 3 and 4 are also essentially different from the results of Larsen & Thorkildsen (1998) which were presented as dashed lines in Fig. 1 of Ro00*b*. This may be regarded as an additional indication for the justification of the conclusions made by Rossmanith (2000*c*), *i.e.* that neither equation (2) of Larsen & Thorkildsen (2000) nor the expression given earlier by Larsen & Thorkildsen (1998) are exact (analytical) expressions for a perfect spherical crystal.

For $\theta_B > 50^\circ$ and large $\bar{t}_{in}/\Lambda$ ratios, the results obtained with B&C's analytical expression considerably exceed the exact solution of the Hamilton–Darwin transfer equations obtained for $\theta_B = 90^\circ$ (curve 3). For $\theta_B > 60^\circ$ these results even exceed curve 2, the absolute upper limit for the t_{ext}/Λ ratio of a spherical crystal [for $\theta_B > 65^\circ$, B&C's expression (37) becomes complex]. For $\theta_B < 20^\circ$, on the other hand, the dashed curves fall below curve 4, the exact result obtained for $\theta_B = 0^\circ$. The deviations between the curves 3 and 4 and the dashed curves are most probably caused by the approximations used for the derivation of B&C's expressions (17), (36) and (37). Similar deviations are observed for the y_p values of Al Haddad & Becker (1990) and Chukhovskii *et al.* (1998), which are based on the more modern dynamical Takagi–Taupin equations (see Fig. 2 of Ro00*b*). Obviously, the deviations are not inherent in the kinematical or dynamical approach. They seem to be caused by the procedure to build up the approximate solution of the transfer equations for intermediate Bragg angles for the boundary conditions of a sphere.

Nevertheless, it is obvious from Fig. 9 that in the case of a moderate Bragg-angle range and small perfect crystallites, *i.e.* for the restrictions of Table 1 of B&C, $\theta < 64^\circ$ and $\bar{t}_{in}/\Lambda \leq 4.2$, the B&C analytical expression for the primary-extinction factor is a valuable tool in routine structure analysis. On the other hand, for large perfect crystal spheres and large Bragg angles, only a poor approximation will be obtained with B&C as well as with the Al Haddad & Becker (1990) and Chukhovskii *et al.* (1998) formalism.

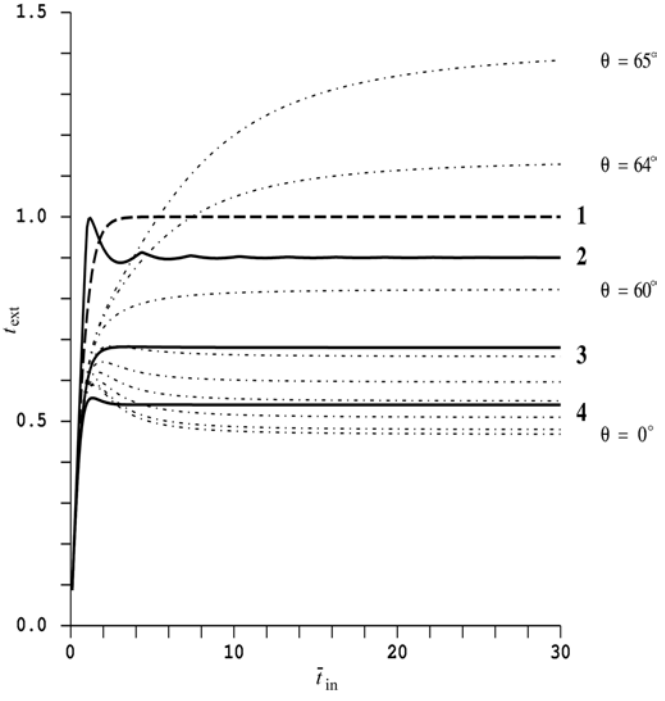

Figure 9
The extinction-corrected mean thickness, $t_{ext} = \bar{t}_{in} y_p$, of the spherical crystal *versus* the mean thickness of the crystal, $\bar{t}_{in}$, for $\Lambda = 1$ (t_{ext}, $\bar{t}_{in}$, Λ in the same arbitrary units). Curve 1: $t_{ext} = \Lambda \tanh(\bar{t}^{\infty}/\Lambda)$. Curve 2: result corresponding to the $R(\zeta)_{upperlimit}$ profiles. Curve 3: result corresponding to B&C's 'Bragg case' profiles. Curve 4: result corresponding to B&C's 'Laue case' profiles. Dashed-dotted curves: obtained with B&C's analytical expression for y_p, calculated for the Bragg angles θ = 0, 10, 20, 30, 40, 50, 60, 64, 65°.

5. Discussion

In the notation defined in the previous sections, the kinematical intensity, I_h, given by A&M for the plane parallel plate in reflection geometry, can be expressed as [A&M's $\Delta\theta$ and $2kt\cos\theta = (2\sin\theta\cos\theta/\lambda)(t/\sin\theta)$ are equivalent to $\omega = \zeta\lambda L$ and $\bar{t}_B^{\infty}/\lambda L$, respectively]

$$I_h = \frac{1}{\sin^2\theta_B}\frac{1}{\Lambda^2}\left(\frac{\sin\pi\bar{t}_B^{\infty}\zeta}{\pi\bar{t}_B^{\infty}\zeta}\right)^2, \qquad (22)$$

an expression similar to (15), the 'kinematical approximation' obtained in the framework of the dynamical theory. I_h has dimensions of cm^{-2}, although the term V^2 in the A&M formula has been replaced in (22) by $1/V^2$, where V is the volume of the unit cell (without this correction the dimensions of the 'kinematical intensity' would be cm^4). The integrated intensity,

$$\int_{-\infty}^{\infty} I_h \,\mathrm{d}\zeta = \frac{1}{\sin^2\theta_B}\frac{1}{\Lambda^2}\frac{1}{t_B^{\infty}}$$

differs appreciably from the crystal-shape-independent expression (4). Furthermore, the FWHM of the kinematical intensity profile given by A&M,

$$\Delta\omega_{FWHM} = \frac{0.44295\lambda}{t_0\cos\theta_B}, \qquad (23)$$

suggests the proportionality of the FWHM to the reciprocal of the cosine of the Bragg angle and to the thickness of the crystal plate normal to the surface, t_0, in apparent disagreement with the shape-independent generally valid expression (7), $\Delta\omega_{integral} = \lambda L/\bar{t}_{diffr}$, where $L \cong 1/\sin 2\theta$ and $\bar{t}_{diffr}$ is the

average thickness of the crystal in the direction of the diffracted beam. Bearing in mind that in the symmetrical Bragg case of the crystal plate with infinite lateral extension $t_0 = t_B^\infty \sin\theta_B$ and that for the profile (22) $\Delta\omega_{\rm FWHM} = 0.88589\Delta\omega_{\rm integral}$ (this relation is obtained by means of *Mathematica*), it can easily be verified that (23) is a very special case of (7), which is only valid for reflecting planes parallel to the infinite surface of a plane parallel crystal plate.

The statement concerning the validity of the Scherrer equation for the crystallite size effect in the case of 'rocking curves' haunts through the literature [see, for example, Sabine (1988; §4); Mathieson (1994; footnote on page 125)]. As emphasized by Rossmanith (1994), however, the Scherrer equation is valid only for the experimental conditions of a powder 2θ scan, which differs essentially from the experimental conditions of a single-crystal ω scan. The factor 0.44295, which is only about half of the Scherrer constant, $K \simeq 1$, is an indication that (23) is not the Scherrer equation.

6. Conclusions

It was shown that the maximum as well as the shapes of the kinematical Bragg intensity profiles depend on a variety of factors: the shape of the crystal, the crystal system and magnitudes of the lattice parameters, the angles between the crystal edges and the unit-cell axes, the angles between the direction of the diffracted beam and the cell axes. Furthermore, it was shown that the widths of the profiles are determined by the Lorentz factor and the mean thickness of the crystal in the direction of the diffracted beam, for all crystal shapes. It was shown that the kinematical reflectivity distribution of a very thin finite plane parallel plate is almost identical to the dynamical profile of a thin plane parallel plate with infinite lateral extension. Considering the extinction-corrected intensity profiles given by B&C for the two special cases ($2\theta = 0$ and 180°), it was concluded that B&C's analytical expression for the primary-extinction correction may be overestimated for large Bragg angles and large perfect crystals.

Note added in proof: Professor A. Authier has pointerd out a copying error in the expression for I_h in Authier & Malgrange (1998), §2.1(iv): V^2 should be replaced by t^2/V^2. An erratum has been published [Authier & Malgrange (2002). *Acta Cryst.* A**58**, 79].

References

Al Haddad, M. & Becker, P. (1990). *Acta Cryst.* A**46** 112–123.
Authier, A. & Malgrange, C. (1998). *Acta Cryst.* A**54**, 806–819.
Azaroff, L. V. (1968). *Elements of X-ray Crystallography.* New York: McGraw-Hill.
Becker, P. J. & Coppens, P. (1974). *Acta Cryst.* A**30**, 129–147.
Chukhovskii, F., Hupe, A., Rossmanith, E. & Schmidt, H. (1998). *Acta Cryst.* A**54**, 191–198.
Larsen, H. B. & Thorkildsen, G. (1998). *Acta Cryst.* A**54**, 511–512.
Larsen, H. B. & Thorkildsen, G. (2000). *J. Appl. Cryst.* **33**, 1447.
Mathieson, A. McL. (1994). *Acta Cryst.* A**50**, 123–126.
Patterson, A. L. (1939). *Phys. Rev.* **56**, 972–977.
Rossmanith, E. (1994). *Acta Cryst.* A**50**, 63–68.
Rossmanith, E. (2000*a*). *J. Appl. Cryst.* **33**, 323–329.
Rossmanith, E. (2000*b*). *J. Appl. Cryst.* **33**, 330–333.
Rossmanith, E. (2000*c*). *J. Appl. Cryst.* **33**, 1448.
Sabine, T. M. (1988). *Acta Cryst.* A**44**, 368–373.
Wilson, A. J. C. (1962). *X-ray Optics.*. New York: John Wiley.
Wolfram, S. (1999). *The Mathematica Book*, 4th ed. Cambridge University Press.
Zachariasen, W. H. (1945). *Theory of X-ray Diffraction in Crystals.* New York: John Wiley.
Zachariasen, W. H. (1967). *Acta Cryst.* **23**, 558–564.